Observation of aluminate whiskers and nanotubes in dynamometer-aged three-way automotive catalysts

Jon Hangas

Ford Motor Company, MD3182, P.O. Box 2053, Dearborn, MI 48121, USA

Received 3 October 2002; accepted 17 December 2002

Short nanotubes and whiskers of aluminates of different compositions, $Ni_xAl_2O_{3+x}$, $SrAl_{12}O_{19}$ and (Nd,La)AlO_3, with a noble metal particle attached to one end, are observed in dynamometer-aged automotive three-way catalysts (TWCs). The samples were from different production formulations for the US market that were aged for 120 h to simulate 100 000 miles of driving with a peak temperature of 1000–1050 °C in the middle of the catalyst monolith. $Ni_xAl_2O_{3+x}$ appears as nanotubes in both Pt/Rh- and Pd-based catalysts with NiO additions. The nanotubes suspend the precious metal catalyst particles in the gas stream. Solid whiskers of $SrAl_{12}O_{19}$ have been found in a Pd-based catalyst with SrO additions in both pores and within alumina agglomerates. (Nd,La)AlO_3 whiskers have thus far been found only within alumina agglomerates in a Pd-based catalyst. The aspect ratio of the whiskers and nanotubes observed after aging is 4 : 1 or more. The solid noble metal particles are cuboctohedral in shape and average 90–150 nm in diameter, depending on the sample. Catalyst particle size controls the nanotube and whisker diameter, although some conical whiskers have also been observed.

KEY WORDS: aluminate whiskers; aluminate nanotubes; aged automotive three-way catalysts.

1. Introduction

Three-way catalysts are used in automobile exhaust systems. They operate near stoichiometry, cycling through rich and lean conditions, to oxidize hydrocarbons and carbon monoxide and to reduce nitrogen oxides. Current designs use a multi-channel extruded cordierite substrates called monoliths on to which porous ceramic washcoat layers containing alumina, ceria or ceria–zirconia (an oxygen storage material) and noble metals are applied [1,2]. Nickel is added to catalysts in the US market for control of H_2S emissions. Sr and rare earths have been added to Pd-based catalysts to make the Pd more resistant to the effects of poisoning by S. Pt/Rh catalysts are intrinsically more resistant to poisoning and do not have as many additives.

Generally in automotive catalysis, specific metal–support combinations are intended by design either to promote a particular interaction (*e.g.*, oxygen release from ceria) or to avoid an unwanted interaction (*e.g.*, the reaction of Rh with alumina). In reality, catalysts are dynamic systems where metal particles move and affect their substrates. Pt particles on alumina have been observed in environmental TEM (transmission electron microscopy) to be mobile at temperatures as low as 430 °C [3]. Pd particles have been observed to cause pits in CeO_2 under high-temperature reducing conditions [4]. Carbon fiber growth from hydrocarbon decomposition has been observed in catalysts made with ceria and alumina [5–7]. However, catalytically assisted ceramic crystal growth has not been reported previously for automotive catalysts, although catalytically assisted growth of fibers (a generic term to include whiskers, which are single crystal, nanotubes, nanowires, filaments, etc.) of carbon and other compounds has been known for decades.

The fibrous materials (i.e. nanotubes, whiskers and polycrystalline fibers) found in this study are generally shorter that the minimum 10 : 1 aspect ratio normally defined as fibers in the engineering community [8], but the growth processes are the same as seen in a type of nanotube growth, as will be discussed below.

2. Experimental

Automotive catalysts of three different proprietary formulations in production for the US market were dynamometer aged for 120 h at elevated temperatures to simulate driving 100 000 miles. The air/fuel ratio was continuously cycled between stoichiometric, rich and lean conditions throughout the accelerated aging. They were aged such that the temperatures at the middle of the catalyst monolith reached a maximum of 1000–1050 °C during the lean portion of the cycle. Formulation A is a Pt/Rh catalyst with Ni but few rare earths, and it reached a maximum of 1050 °C. Formulations B and C are both two-layer Pd-based catalysts containing Sr, Ba, La, Nd and Ni that were aged at a maximum of 1000 °C.

The catalyst monoliths were cut and cores about 3 cm long were removed. TEM samples were made from

* To whom correspondence should be addressed.

1011-372X/03/0300-0267/0

material a consistent distance from the inlet of each monolith. Crushed powder samples for TEM were made by scraping washcoat off the cordierite monolith support, crushing the powder between glass slides, dipping a holey carbon grid into the powder and then carbon coating. Cross-sections for TEM were prepared by impregnating in Gatan G-1 epoxy, tripod polishing at a 2° wedge angle and low-angle ion milling in a Gatan PIPS with a beam of 3 keV or less. A JEOL 2000 FX TEM with an Oxford Instruments AN10 EDX (energy-dispersive X-ray) system was used for analysis. In some cases fresh catalysts of the same formulations were examined in cross-section.

3. Results

The general microstructure of the lower washcoat of formulation A consists mostly of alumina agglomerates [figure 1(a)]. Epoxy still fills most of the cracks and pores between the agglomerates but has been milled away in the thinner regions. The thickness of the foil increases gradually from the top to the bottom of the image. Pt/Rh particles are observed between agglomerates, in small pores in agglomerates, and a few are in the middle of the alumina agglomerates. The Pt/Rh particles in between the agglomerates are usually suspended on nanotubes of $Ni_xAl_2O_{3+x}$ [figure 1(b)]. The microdiffraction pattern in the inset is of the [111] zone axis, and was taken at the point marked N. Extra spots in this diffraction pattern may be due to faults within the area excited by the beam. The [11$\bar{2}$] direction is parallel to the projection of the growth direction of this segment of the nanotube. EDX determined that this whisker had about 3.5 wt% Ni, corresponding to a molecular formula of $Ni_{0.06}Al_2O_{3.06}$. The Ni content was observed to vary from 1 to 8 wt% (x ranged from 0.02 to 0.15) in 10 nanotubes examined in this sample. The nanotubes are probably a solid solution between γ-Al_2O_3 and $NiAl_2O_4$ spinel in composition. Small

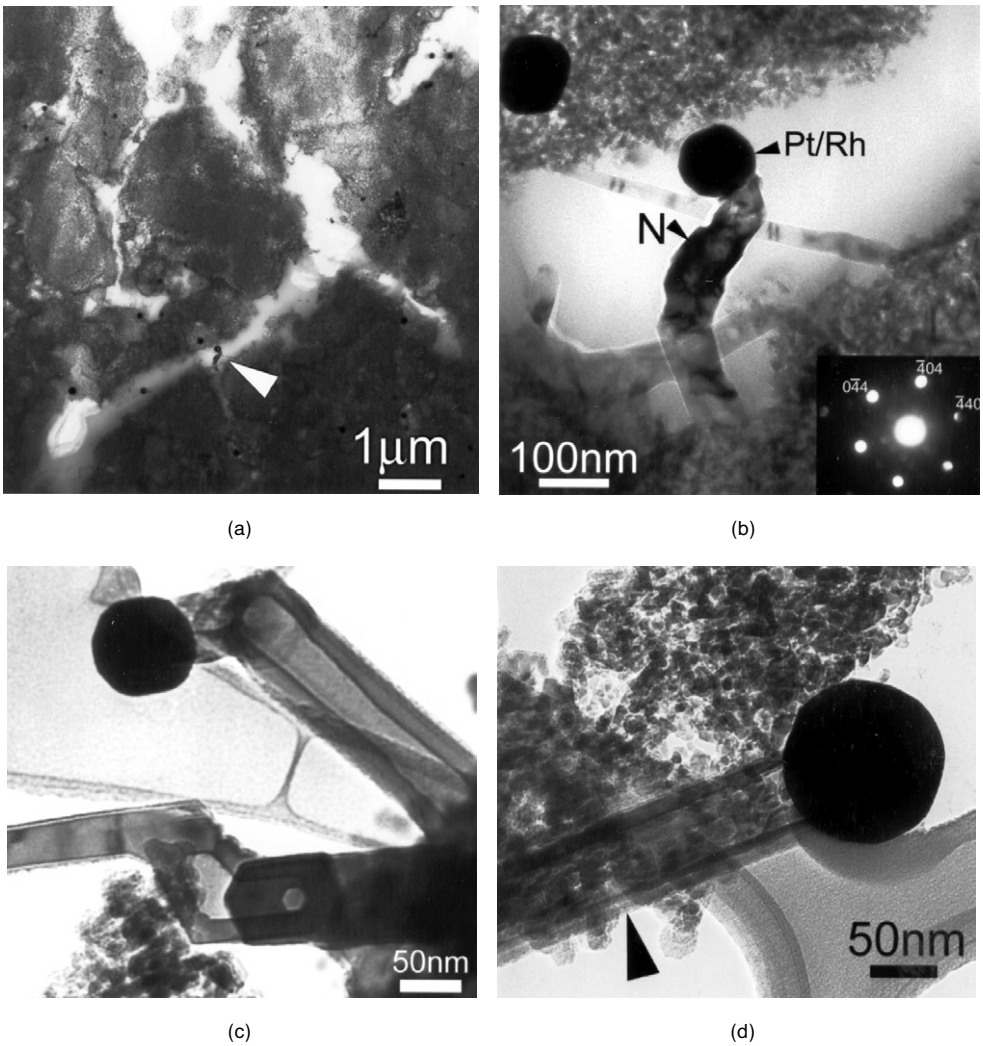

Figure 1. (a) TEM cross-section of formulation A. Most Pt/Rh particles are between agglomerates. The arrow points to the area of (b) where a $Ni_xAl_2O_{3+x}$ nanotube (N) is growing in a crack between alumina agglomerates. The inset shows the [111] zone axis microdiffraction pattern taken from the segment marked by the arrow N. (c, d) Nanotubes from a crushed powder sample of formulation A.

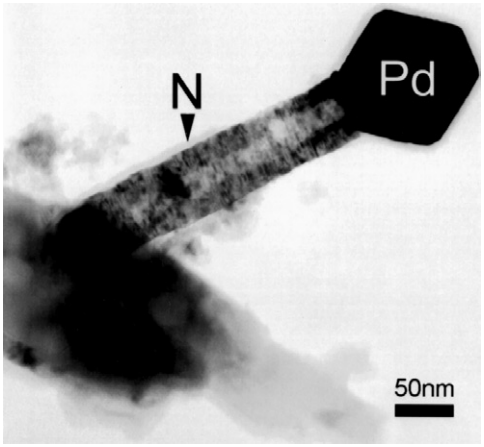

Figure 2. $Ni_xAl_2O_{3+x}$ nanotube (N) attached to Pd particle and a larger crystal of $Mg_{0.5}Ni_{0.5}Al_2O_4$ at the lower left. The Pd particle is at the [110] zone axis and [001] is roughly parallel to the nanotube growth direction. The {111} Pd faces are well developed at the expense of {110}.

amounts of Si are detected in EDX, but most of this is presumably from stray radiation. Two other nanotubes of $Ni_xAl_2O_{3+x}$ cross the crack, but the particles that grew them were removed in the cross-sectioning process. The nanotubes are attached to the alumina agglomerate, but these may not be the points of nucleation, since those may also be out of the foil. Some nanotubes [figure 1(c)] from this formulation appeared to be almost single-crystal tubes with jogs, with slight variations in wall thickness. Nanotubes with thinner walls exist [figure 1(d)]. The predominant morphology tends toward more irregular shapes as in figure 1(b). Only $Ni_xAl_2O_{3+x}$ or $(Mg,Ni)_xAl_2O_{3+x}$ nanotubes were found in formulation A. The nanotubes with Mg in solid solution are found within a few microns of the cordierite. The Mg is assumed to have been from excess MgO added to the cordierite.

A nanotube of $Ni_xAl_2O_{3+x}$ from a crushed powder sample of Pd-based formulation B is shown in figure 2. The Pd particle is oriented to its [110] zone, and the Pd (001) plane is the base on which this particle is attached to this nanotube. The projection of the nanotube growth direction is also parallel to the $[11\bar{2}]$ direction as in figure 1(b), as determined from a [111] microdiffraction pattern. The wavy contrast present in the nanotube may be due to either thickness changes or local strains introduced during growth as the Pd tilts back and forth. The uniform diameter of the nanotube suggests that the Pd particle had already reached its current size when its motion carried it into contact with the large $Mg_{0.5}Ni_{0.5}Al_2O_4$ spinel grain on which the $Ni_xAl_2O_{3+x}$ nanotube appears to have nucleated. This is the only occasion where a $Mg_{0.5}Ni_{0.5}Al_2O_4$ spinel has been observed in this catalyst, and it may have formed from a reaction between an agglomerate of NiO (previously observed to line the pores in the fresh material), alumina, and excess MgO from the cordierite.

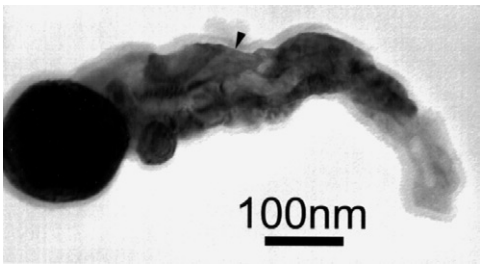

(a)

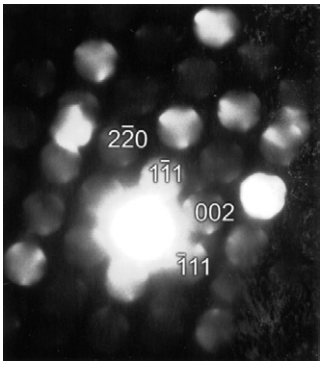

(b)

Figure 3. (a) Conical whisker of $Ni_xAl_2O_{3+x}$ with a Pd particle attached at left. The carbon coating is visible around most of the fiber. (b) [110] zone microdiffraction pattern from a small crystallite almost 100 nm long marked by the arrow at the top center of (a) at another orientation of the whisker.

There are few $Ni_xAl_2O_{3+x}$ nanotubes observed in formulation B as straight as that in figure 2. Conical whiskers are occasionally observed (figure 3), and microdiffraction was done on one to confirm it was $Ni_xAl_2O_{3+x}$. There was more than one orientation variant in this whisker, but it was not determined if these were twin related or whether this whisker would be more appropriately called a polycrystalline fiber. It may also have a hollow core in places. Most nanotubes have very thin walls, as in figure 4. These nanotubes are growing adjacent to a zirconia–ceria agglomerate in formulation C. This morphology may appear when the nanotube is not getting as good a supply of NiO and Al_2O_3 to grow as the nanotube in figure 2. The nucleation points of such nanotubes were never confirmed in cross-section.

Whiskers of $SrAl_{12}O_{19}$ were also found growing both in pores and within alumina agglomerates in formulation B (figure 5). The $SrAl_{12}O_{19}$ whiskers appear to have a conical shape. The more massive whiskers found in the crushed powder sample may have grown from an agglomerate rich in SrO, which has been found in the fresh catalyst material. Figure 5(a) was taken at the Pd [110] zone axis, which is just a few degrees from the hexagonal $SrAl_{12}O_{19}$ $[1\bar{2}0]$ zone [figure 5(b)] and still clearly shows the *c*-axis lattice fringes in the whisker. This whisker appears to be a single crystal with its *c*-axis

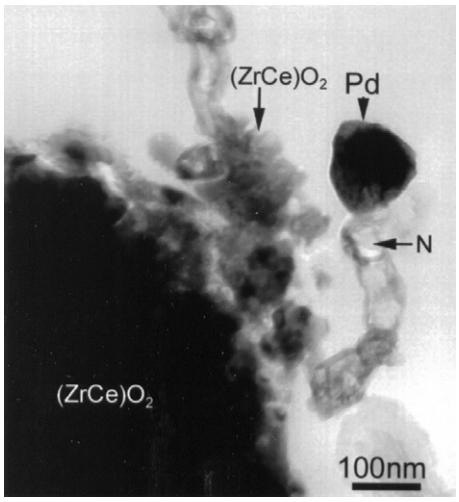

Figure 4. A thin-walled, irregular nanotube of $Ni_xAl_2O_{3+x}$ (marked by arrow N) growing next to a zirconia–ceria agglomerate in a cross-section from formulation C. The image is from a tripod polished cross-section, and the irregular shape of the Pd may be due to thinning damage.

roughly parallel to the growth direction. This Pd particle has an orientation relationship within a few degrees of $[1\bar{1}1]_{Pd}||[001]_{whisker}$ and $[110]_{Pd}||[1\bar{2}0]_{whisker}$. Other $SrAl_{12}O_{19}$ whiskers have been observed to have at least two orientation variants in contact with the catalyst particle. The Pd particle shape appeared consistent with both orientation variants having their basal planes parallel to a Pd (111) plane.

An $SrAl_{12}O_{19}$ whisker containing Ba has been observed. $SrAl_{12}O_{19}$ and $BaAl_{12}O_{19}$ have the same lattice parameters but have different structures and are insoluble with each other and Al_2O_3 at 1400 °C [9]. The whisker may contain the Ba and Sr in different layers, instead of solid solution. Typically $BaAl_2O_4$ has been observed in other catalyst materials containing Ba, but no $BaAl_2O_4$ or $BaAl_{12}O_{19}$ whisker formation has been observed.

Whisker growth can also occur owing to particle motion within an alumina agglomerate that contains

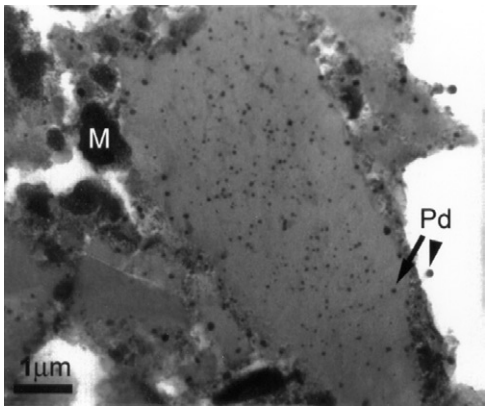

(a)

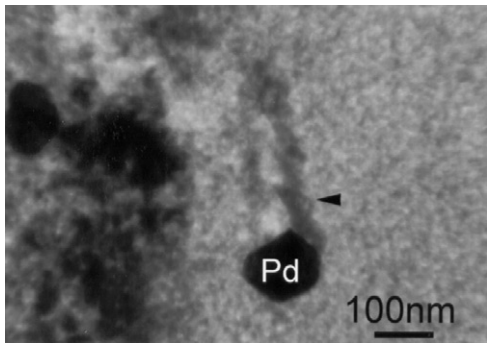

(b)

Figure 6. Cross-section TEM image of the outer washcoat of formulation B. (a) The outer washcoat with the free surface of the washcoat at right. (b) Pd particle which left a trail consistent with $SrAl_{12}O_{19}$ (marked by the arrow) in the alumina agglomerate in (a), as determined by EDX. The mottled background is due to the small crystallite size of the alumina.

the necessary additives. Whiskers consistent with $SrAl_{12}O_{19}$ were found within alumina agglomerates in formulation B (figure 6). The outside surface of the outer washcoat is heavily impregnated with Pd [figure 6(a)]. There are also dark agglomerates of ceria-zirconia

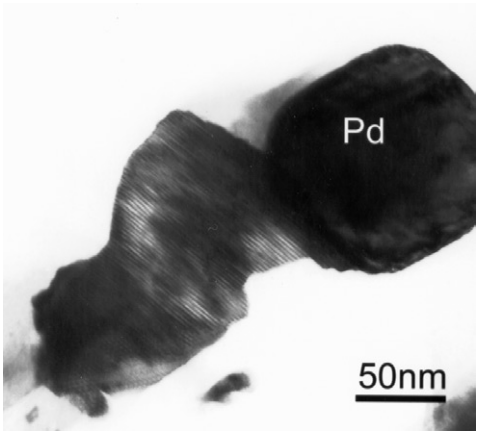

(a)

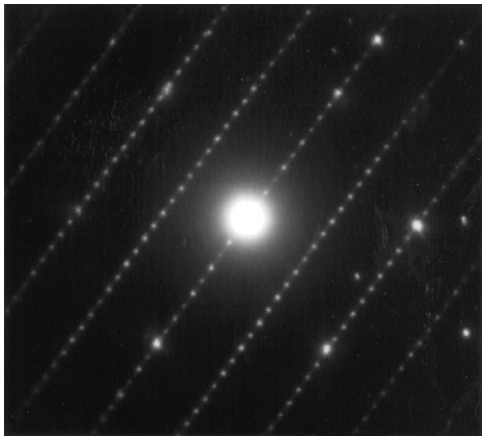

(b)

Figure 5. TEM images of $SrAl_{12}O_{19}$ whiskers from a crushed powder sample of formulation B. (a) Whisker attached to Pd particle, with (b) $[1\bar{2}0]$ SAD pattern. The SAD pattern also includes some reflections from the Pd particle, which indicates that the Pd is only a few degrees from its [110] zone axis.

(marked "M"). A higher magnification view [figure 6(b)] shows that all the small equiaxed particles within the alumina agglomerate at the center of (a) are Pd particles. Many have thin whiskers of $SrAl_{12}O_{19}$ growing on them, but this was determined by EDX spectroscopy only, owing to the difficulty of tilting the thin crystals. Morphology suggests that instead of growth being parallel to the hexagonal $[001]_{whisker}$ axis, it is highly inclined with growth occurring by the Pd particle gliding across $(0001)_{whisker}$ plane in the same direction. There are also small voids next to the whisker in the wake of the particle. Some Pd is also visible in pores or on the top surface. The small, round particles within the alumina agglomerate at the center of the figure are Pd particles. Some Pd particles are on whiskers on the outer surface or in pores.

Whiskers of $(Nd,La)AlO_3$ were found to occur in alumina agglomerates in formulation C (figure 7). These were identified by both electron diffraction and EDX. The conical whisker in figure 7(a) is attached to a Pd particle. The contact point between the straight whisker marked Nd and the Pd particle above it in figure 7(b) has been removed by the sample preparation process. This whisker appears to branch off another crystal.

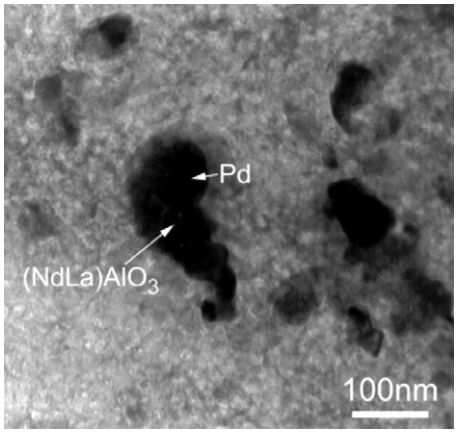

(a)

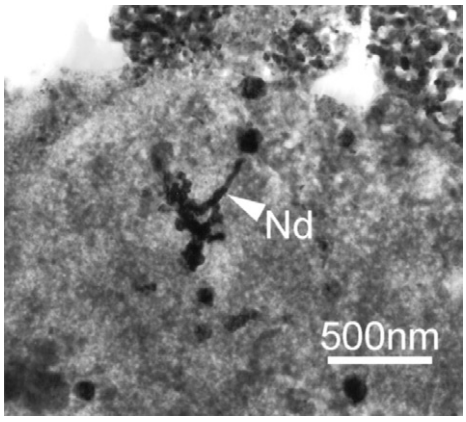

(b)

Figure 7. (a) A short conical $(Nd,La)AlO_3$ whisker with Pd particle attached that grew in an alumina agglomerate in formulation C. (b) Longer straight whiskers are also found.

4. Discussion

Carbon nanotubes can be grown by arc discharge, laser ablation and chemical vapor deposition techniques. Laser ablation has been used to grow nanotubes where the graphite target is doped with small amounts of Ni/Co, Rh/Pd or Pt/Rh catalyst [10]. Catalyst particles are solid during the nanotube growth process, and appear equiaxed. The catalyst does not have to exothermically decompose a fuel gas, and carbon diffusion would be by surface diffusion.

In growth of carbon nanotubes or amorphous carbon fibers by CVD (chemical vapor deposition) or fuel gas decomposition, an exothermic reaction occurs on the top surface of the particle. Bulk diffusion of carbon is necessary to separate it from other elements of the fuel gas, and graphitic carbon precipitates out on the cooler substrate side of the particle where fiber growth occurs [11]. The combination of the heat from the exothermic reaction and the bulk diffusion produces catalyst particles that are elongated or teardrop shaped, with frequent particle fragmentation that produces branched fibers.

The vapor–liquid–solid (VLS) method is a CVD technique that uses a liquid catalyst particle on to which the vapor phase condenses and precipitates out in the form of a whisker [12]. VLS has been used to grow whiskers such as SiC [13], SiO_2, Si_3N_4 and ZnO [14]. Vapor–solid (VS) growth uses no catalyst, but requires a crystal defect such as a screw dislocation to be present for growth to occur.

In this study, the catalyst particles are solid. The melting-point of Pd is 1555 °C, and the Pt–Rh alloy would have a melting-point at least 200 °C higher. A liquid catalyst particle cannot produce a nanotube like the $Ni_xAl_2O_{3+x}$ nanotubes that have been observed. Bulk diffusion of Al, Ni, Sr, La and Ba through the catalyst particle is also energetically unfavorable. Growth of carbon nanotubes by laser ablation is the only fiber growth process that uses solid catalysts without bulk diffusion. Vapor phase is the dominant means of transport to those fibers located in pores, whereas those growing in alumina grains can also have material by surface or intergranular diffusion. Agglomerates of NiO and SrO are known to be present in the fresh catalyst of formulation B. The identity of the chemical compounds leading to vapor transport of Ni and Sr is not known.

The catalyst particle size controls the diameter of the whiskers and nanotubes. Conical whiskers nucleated when the particle was relatively small, and grew in diameter as the particle grew. The $Ni_xAl_2O_{3+x}$ nanotube

wall thickness remains fairly constant in an individual nanotube, but there is a range of distribution in thickness between different nanotubes. The wall thickness may be dependent on the wall thickness at the point of nucleation, as well as temperature and availability of Ni and Al. The relatively constant wall thickness suggests that there is no evidence for either significant ablation of material with time or for significant additional deposition of material to the sides of the nanotube by the VS process increasing the diameter with time. It is not known whether all Ni has been incorporated into $Ni_xAl_2O_{3+x}$ upstream of where the cross-sections were made. It is not known why significant nanotube growth did not occur when the average particle size was smaller, or whether it was not preserved.

Anchoring particles on fibers such as the whiskers and nanotubes in this study can be one method to discourage exaggerated particle growth by coalescence, even if fiber nucleation is delayed. The author has found particles up to 1 μm in diameter in a vehicle-aged catalyst that had only trace amounts of Ni or Sr added. Many additional unresolved questions remain that would have to be solved by model catalyst samples or additional dynamometer runs under different conditions. These include time and temperature of nucleation, transport species and the rate at which growth continues, if at all, after the additives are fully incorporated into aluminates. Better dispersion of the Ni and other additives may lower the nucleation size of the fibers.

5. Conclusion

Aluminate nanotubes and whiskers have been found in two Pd-based and one Pt/Rh fully formulated automotive catalysts that were dynamometer aged at 1000–1050 °C. Growth of $Ni_xAl_2O_{3+x}$ nanotubes occurred in all three catalysts. $SrAl_{12}O_{19}$ whiskers were observed in a Pd catalyst to grow both in pores and in alumina agglomerates where surface diffusion is a possible transport means. (Nd,La)AlO_3 was only observed in alumina agglomerates in another Pd-based catalyst. The growth mechanism is thought to be analogous to growth of carbon nanotubes by laser ablation using solid catalyst particles.

Acknowledgments

The author thanks Charlotte Lowe-Ma for the many helpful discussions and George Graham and Bill Donlon for their encouragement, insightful suggestions and critical reading of the manuscript. Charlotte Lowe-Ma, Dave Benson, Ann Chen and Michellene Peck all contributed to the overall understanding of these catalyst materials.

References

[1] M. Shelef and R.W. McCabe, Catal. Today 62 (2000) 35.
[2] H.S. Ghandi, G.W. Graham and R.W. McCabe, J. Catal. submitted.
[3] E.G. Bithell, R.C. Doole, M.J. Goringe and G.M. Parkinson, Inst. Phys. Conf. Ser. No. 138: Section 10 (1993) 461.
[4] L. Kepinski and M. Wolcryz, Appl. Catal. A: Gen. 150 (1997) 197.
[5] L. Kepinski, Catal. Today 50 (1999) 237.
[6] J. Hangas, Microsc. Microanal. 6 (Suppl. 2: Proceedings) (2000) 66.
[7] A. Thaib, G.A. Martin, P. Pinheiro, M.C. Schouler and P. Gadelle, Catal. Lett. 63 (1999) 135.
[8] H.W. Rauch, Sr., W.H. Sutton and L.R. McCreight, Technical Report AFML-TR-68-162, General Electric Company, September, 1968.
[9] P. Appendino, Rev. Int. Hautes Temp. Réfrac. 9 (1972) 297.
[10] T. Gennett, A.C. Dillon, J.L. Allerman, K.M. Jones, P.A. Parilla and M.J. Heben, Mater. Res. Soc. Symp. Proc. 633 (2001) A2.3.1.
[11] R.T.K. Baker, Carbon 27 (1989) 315.
[12] R.S. Wagner and W.C. Ellis, Appl. Phys. Lett. 4 (1964) 89.
[13] S.R. Nutt, J. Am. Ceram. Soc. 71 (1988) 149.
[14] H. Cui, W. Liu and B.R. Stoner, Mater. Res. Soc. Symp. Proc. 633 (2001) A13.42.1.